arXiv:1512.07816v1 [nucl-th] 24 Dec 2015

Unified description of rotational-, γ-, and quasiparticle-band structures in neutron-rich mass $\sim$ 110 region

G. H. Bhat[1], J. A. Sheikh[1], Y. Sun[2,3,4], and R. Palit[5]

[1] *Department of Physics, University of Kashmir, Srinagar, 190 006, India*
[2] *Department of Physics and Astronomy, Shanghai Jiao Tong University, Shanghai 200240, People's Republic of China*
[3] *Collaborative Innovation Center of IFSA (CICIFSA), Shanghai Jiao Tong University, Shanghai 200240, People's Republic of China*
[4] *State Key Laboratory of Theoretical Physics, Institute of Theoretical Physics, Chinese Academy of Sciences, Beijing 100190, People's Republic of China*
[5] *Department of Nuclear and Atomic Physics, Tata Institute of Fundamental Research, Colaba, Mumbai, 400 005, India*

Abstract

Band structures of the neutron-rich Mo- and Ru-isotopes around A $\sim$ 110 are investigated using the triaxial projected shell model (TPSM) approach employing multi-quasiparticle configuration space. The mass region under investigation depicts a rich variety of band structures with well developed γ- and $\gamma\gamma$-bands, and quasiparticle excitations based on them. It is demonstrated that TPSM provides a reasonable description of most of the observed properties, in particular, detailed structure variations observed in Mo-isotopes are well reproduced in the present work.

Key words: , γ-vibrations, quasiparticle excitations, triaxial projected shell model
PACS: 21.60.Cs, 21.10.Hw, 21.10.Ky, 27.50.+e

1 Introduction

The basic modes of nuclear excitations are of rotational, vibrational, and multi-quasiparticle (qp) in character and in many regions of nuclear periodic table these three modes coexist. One of the major challenges to nuclear models is to provide a unified description of these basic excitation modes. There is a long history of phenomenological models that were introduced to study the interplay among the three modes of excitations [1,2,3,4]. On the

microscopic front, however, there are very few models capable of describing the three modes of excitations in a unified manner, in particular, at higher angular momenta.

Nuclei around A $\sim$ 110 exhibit some of the most interesting features in the nuclear periodic table. For instance, many nuclei in this region depict quite large deformation with $\beta \sim 0.45$, which is understood as due to the reinforcing effect of proton and neutron deformed shell gaps at $Z = 38$, 40 and $N = 60$, 62 [5,6,7,8,9]. Further, in some nuclei in this region, well developed γ- and $\gamma\gamma$-bands have been observed up to quite high angular momenta. For example, γ- and $\gamma\gamma$- bands have been identified in $^{104-106}$Mo isotopes [10,11,13,12]. Although yrast bands in this mass region have been studied using theoretical approach of total routhian surface model [5,7,8,14,15,16,17,18], there appears no systematic investigation of the γ-bands.

Microscopic triaxial projected shell model (TPSM) approach [19] has been developed and it has been demonstrated to provide a coherent and accurate description of yrast-, γ- and $\gamma\gamma$-bands in deformed nuclei [20]. In this approach, the three dimensional angular-momentum projection operator is employed to project out the good angular-momentum states from triaxially-deformed Nilsson + BCS basis. The shell model Hamiltonian is then diagonalized using these angular-momentum projected basis states. This model was initially restricted to perform the projection from the vacuum configuration only and it was possible to study only low-spin states [20,21,22,23,24]. The model space has now been expanded by including multi-qp states above the triaxially-deformed qp vacuum and it is now possible to extend the study of yrast and other band structures to high-spin states [25,26].

The multi-qp TPSM approach has been employed to investigate the high-spin band structures in Er-isotopes and in the mass $A \sim 130$ region. It has been shown in some Er-isotopes that γ-bands built on the two-qp configurations can become yrast at higher angular-momenta [25]. In the mass $A \sim 130$ region, the TPSM model has provided an alternative explanation of a long-standing puzzle of two-aligned bands with identical intrinsic configuration observed in some nuclei. It has been shown that the two observed aligned states in ^{134}Ce, having identical neutron configuration, are the normal two-qp neutron aligned band and the γ-band built on this configuration [26].

Recently, we have further generalized the TPSM approach to study the γ-vibration in odd-proton nuclei and a preliminary application of this new development for ^{103}Nb has already been reported [27]. In the present work, we have also developed TPSM model for odd-neutron systems and would like to investigate the observed γ-vibrational band structures in the mass $A \sim 110$ region where rich band structures are observed in odd-neutron systems. This is one of the few mass regions in the periodic table where ground-state axial-

shape-asymmetry is suggested [28], and also where γ- and $\gamma\gamma$- bands have been identified in odd-mass ^{105}Mo nucleus up to quite high angular momenta [14,12,30,29]. The purpose of the present work is to perform a systematic study of the band structures observed in these nuclei and, more importantly, to evaluate the transition probabilities using the extended version of the TPSM approach.

The manuscript is organized as follows : In the next section, we shall provide a brief sketch of the multi-qp TPSM approach, in particular, we shall provide a few details on the multi-qp basis states employed in the present analysis. In section III, the results of our calculations for even-even and odd-neutron systems are presented and discussed in two subsections. Finally, the present work is summarized in section IV.

2 Triaxial Projected Shell Model Approach

In the present work, the TPSM calculations are performed for even-even and odd-neutron isotopes. For the even-even system, the TPSM basis is composed of 0-qp vacuum, two-proton, two-neutron and four-qp configurations, i.e.,

$$\begin{aligned} \hat{P}^I_{MK} \,|\, \Phi > ; \\ \hat{P}^I_{MK}\ a^\dagger_{p_1} a^\dagger_{p_2} \,|\, \Phi > ; \\ \hat{P}^I_{MK}\ a^\dagger_{n_1} a^\dagger_{n_2} \,|\, \Phi > ; \\ \hat{P}^I_{MK}\ a^\dagger_{p_1} a^\dagger_{p_2} a^\dagger_{n_1} a^\dagger_{n_2} \,|\, \Phi > \ . \end{aligned} \tag{1}$$

For the study of odd-neutron system, our model space is spanned by the following angular-momentum-projected one- and three-qp basis :

$$\begin{aligned} \hat{P}^I_{MK}\ a^\dagger_{n} \,|\, \Phi > ; \\ \hat{P}^I_{MK}\ a^\dagger_{n} a^\dagger_{p1} a^\dagger_{p2} \,|\, \Phi > , \end{aligned} \tag{2}$$

where the three-dimensional angular-momentum projection operator is given by [31]

$$\hat{P}^I_{MK} = \frac{2I+1}{8\pi^2} \int \, d\Omega \, D^I_{MK}(\Omega) \, \hat{R}(\Omega), \tag{3}$$

with

$$\hat{R}(\Omega) = e^{-\imath\alpha \hat{J}_z} e^{-\imath\beta \hat{J}_y} e^{-\imath\gamma \hat{J}_z}, \tag{4}$$

and $|\Phi>$ represents the triaxially-deformed qp vacuum state. It is important to note that for the case of axial symmetry, the qp vacuum state has $K = 0$ [32], whereas, in the present case of triaxial deformation, the vacuum state is a superposition of all possible K-values. Rotational bands with the triaxial basis states, Eqs. (1,2), are obtained by specifying different values for the K-quantum number in the angular-momentum projector in Eq. (3). The allowed values of the K-quantum number for a given intrinsic state are determined through the following symmetry consideration. For $\hat{S} = e^{-\imath\pi\hat{J}_z}$, we have

$$\hat{P}^I_{MK}\,|\Phi\rangle = \hat{P}^I_{MK}\hat{S}^\dagger\hat{S}\,|\Phi\rangle = e^{\imath\pi(K-\kappa)}\hat{P}^I_{MK}\,|\Phi\rangle\,. \tag{5}$$

The qp basis chosen above is adequate to describe high-spin states up to $I \sim 20\ \hbar$ for even-even system, $I \sim 35/2\ \hbar$ for odd-mass nuclei. In the present analysis we shall, therefore, restrict our discussion to this spin regime. For the self-conjugate vacuum or 0-qp state, $\kappa = 0$ and, therefore, it follows from the above equation that only $K =$ even values are permitted for this state. For 2-qp states, $a^\dagger a^\dagger\,|\Phi\rangle$, the possible values for K-quantum number are both even and odd, depending on the structure of the qp state. For example, for a 2-qp state formed from the combination of the normal and the time-reversed states $\kappa = 0$, only $K =$ even values are permitted. For the combination of the two normal states, $\kappa = 1$ and only $K =$ odd states are permitted. For one-qp state, $\kappa = 1/2$ $(-1/2)$, and the possible values of K are $1/2, 5/2, 9/2, \ldots$ $(3/2, 7/2, 11/2, \ldots)$ that satisfy Eq. (5).

As in the earlier PSM calculations, we use the pairing plus quadrupole-quadrupole Hamiltonian [32]

$$\hat{H} = \hat{H}_0 - \frac{1}{2}\chi\sum_\mu \hat{Q}^\dagger_\mu\hat{Q}_\mu - G_M\hat{P}^\dagger\hat{P} - G_Q\sum_\mu \hat{P}^\dagger_\mu\hat{P}_\mu. \tag{6}$$

The corresponding Nilsson Hamiltonian, which is used to generate the triaxially-deformed mean-field basis and can be obtained by using the Hartree-Fock-Bogoliubov (HFB) approximation, is given by

$$\hat{H}_N = \hat{H}_0 - \frac{2}{3}\hbar\omega\left\{\epsilon\ \hat{Q}_0 + \epsilon'\ \frac{\hat{Q}_{+2} + \hat{Q}_{-2}}{\sqrt{2}}\right\}. \tag{7}$$

Here $\hat{H}_0$ is the spherical single-particle Hamiltonian, which contains a proper spin-orbit force [33]. The interaction strengths in (6) are taken as follows: The QQ-force strength χ is adjusted such that the physical quadrupole deformation is obtained as a result of the self-consistent mean-field HFB calculation [32]. The monopole pairing strength G_M is of the standard form

$$G_M^n = \frac{G_1 - G_2 \frac{N-Z}{A}}{A} \text{ for neutrons,} \qquad (8)$$
$$G_M^p = \frac{G_1}{A} \text{ for protons.}$$

In the present calculation, we take $G_1 = 16.22$ and $G_2 = 22.68$, which approximately reproduce the observed odd-even mass difference in the studied mass region. This choice of G_M is appropriate for the single-particle space employed in the model, where three major shells are used for each type of nucleons: i.e. $N = 3, 4, 5$ for neutrons and $= 2, 3, 4$ for protons. The quadrupole pairing strength G_Q is assumed to be proportional to G_M, and the proportionality constant being fixed as 0.18. These interaction strengths are consistent with those used earlier for the same mass region [34].

3 Results and Discussions

The TPSM calculations have been performed for neutron-rich even-even and odd-neutron Mo- and Ru-isotopes which depict γ-band structures. The calculations proceed in several stages. In the first stage, the deformed basis are constructed from the solutions of the triaxially-deformed Nilsson potential. The potential is solved for each nucleus with the axial and triaxial deformation parameters, ϵ and ϵ'. The axial deformation parameter ϵ is normally chosen from the measured quadrupole moment of the system, wherever available, otherwise the tabulated values [35] using the phenomenological potential models are employed. The value of ϵ' is, preferably, chosen from the minimum of the potential energy surface (PES) of the nucleus. However, for some nuclei, PES depicts γ-softness, and for these nuclei the value of ϵ' that reproduces the γ-band head energy is adopted since it is known that this band head energy is very sensitive to the non-axial deformation. In the second stage, standard BCS equation is solved for the monopole pairing interaction with the parameters mentioned earlier. This defines the qp basis of our model. In the next step, states with good angular-momentum are projected out from the qp states using the explicit three-dimensional angular-momentum projection operator. In the final stage, the projected basis is used to diagonalize the shell model Hamiltonian consisting of pairing plus quadrupole-quadrupole interaction terms in Eq. (6). In the following subsections, we shall separately present and discuss the results for even-even and odd-neutron systems.

Table 1
Axial and triaxial quadrupole deformation parameters ϵ and γ (defined by $\tan^{-1}\gamma = \epsilon'/\epsilon$) employed in the TPSM calculation for even-even Mo and Ru isotopes.

	^{102}Mo	^{104}Mo	^{106}Mo	^{108}Mo	^{108}Ru	^{110}Ru	^{112}Ru
ϵ	0.315	0.320	0.310	0.294	0.280	0.290	0.289
γ	25	22	20	25	29	28	25

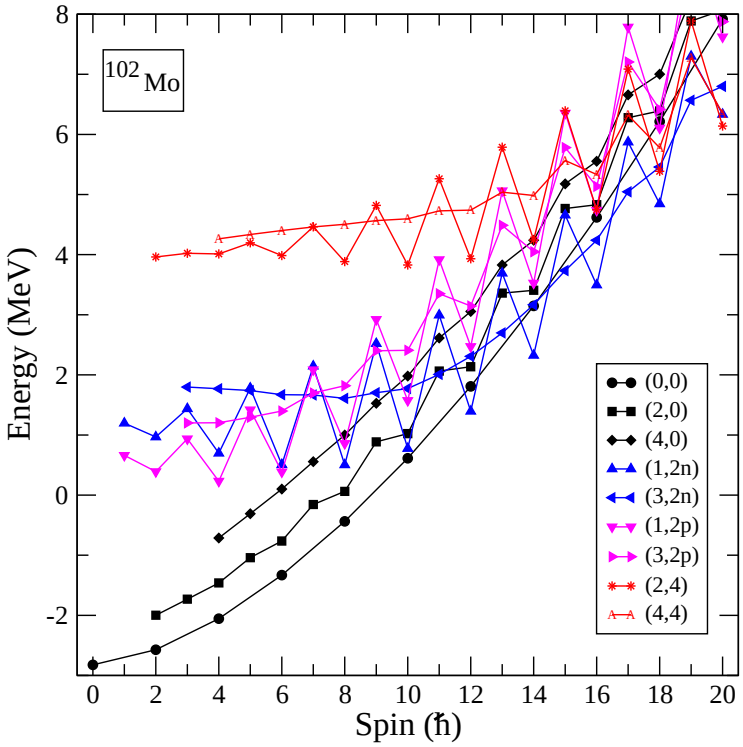

Fig. 1. (Color online) Band diagram for ^{102}Mo. The labels (0,0), (2,0), (4,0), (1,2n), (3,2n), (1,2p), (3,2p), (2,4), and (4,4) correspond, respectively, to the configurations of ground, γ, 2γ, two neutron-aligned, γ-band built on this two neutron-aligned state, two proton-aligned, γ-band built on this two proton-aligned state, two-neutron plus two-proton aligned band, and γ-band built on this four-qp state.

3.1 Even-Even Systems

For even-even systems, we have carried out TPSM calculations for $^{102-108}$Mo and $^{108-112}$Ru isotopes. The axial and triaxial deformation parameters ϵ and γ used for these nuclei are listed in Table 1. The axial deformations have been chosen from the earlier studies [36,37,38,39] and triaxial deformations are chosen, as already mentioned earlier, in such a way that the bandhead of the γ-bands is reproduced.

The basis space for even-even systems is composed of 0-qp, two-quasineutron, two-quasiproton and two-quasineutron plus two-quasiproton configurations as

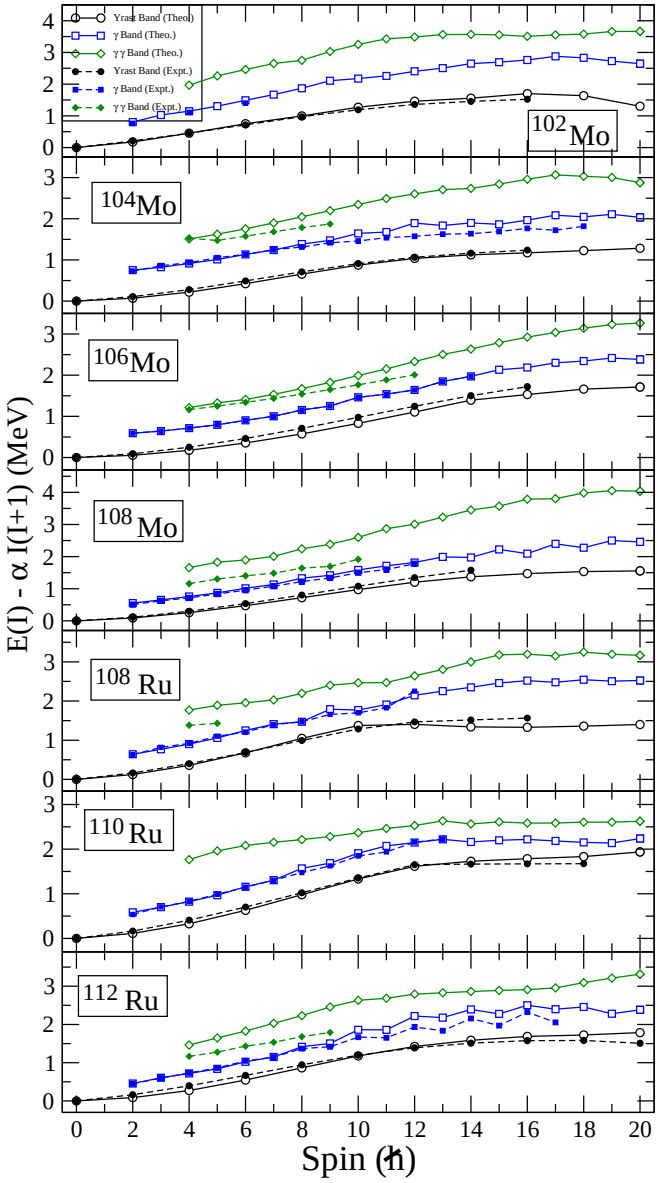

Fig. 2. (Color online) Comparison of the measured energy levels of Yrast-, γ-, and $\gamma\gamma$-bands for ^{102,104,108}Mo and ^{108,110}Ru nuclei and the results of TPSM calculations. The scaling factor α appearing in the y-axis is defined as $\alpha = 32.32A^{-5/3}$. Data are taken from Refs. ([11,12,13,41,42].

given in Eq. (1). The projected bands from 0-qp configuration has $\kappa = 0$ and the allowed values for the projected configurations are $K = 0, 2, 4, \ldots$. The projected band for $K = 0$ constitutes the main component of the ground-state band of an even-even system and the projected bands from $K = 2$ and $K = 4$ correspond to the main components of the γ- and $\gamma\gamma$-band, respectively. The projected bands from two-qp states can have either $\kappa = 0$ or 1. The configurations with $\kappa = 0$ do not become favored for the spin-regime studied in the present work and, therefore, have been disregarded. However, the two-qp configurations with $\kappa = 1$, referred to as the aligned states, become yrast at

higher angular-momenta. As an illustrative example, Fig. 1 depicts the projected energies before configuration mixing from different qp configurations for ^{102}Mo. This figure, referred to as the band diagram [40], is quite instructive to unravel the intrinsic structures of the rich band structures observed in rotating nuclei. To simplify the discussion on such diagrams, the bands are labeled by the symbol $(K, \#t)$, where "K" is the projection of angular momentum in the intrinsic frame and the symbol "#" denotes the number of qps with $t = n(p)$ for neutrons (protons). The ground-state band in Fig. 1, as expected, has the configuration $(0, 0)$ and is crossed by the two-neutron aligning state $(1, 2n)$ at angular momentum $I = 12$. Although the two-proton aligned band, $(1, 2p)$, is almost at the same excitation energy as that of $(1, 2n)$ at lower angular momenta, it does not cross the ground-state band. Bandheads of γ- and $\gamma\gamma$-bands are at excitation energies of 0.83 MeV and 2.11 MeV, respectively.

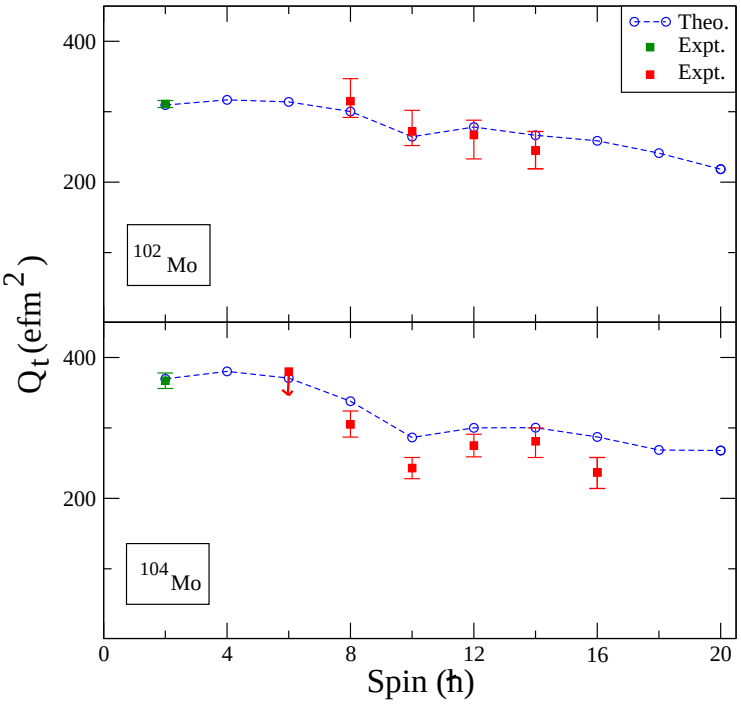

Fig. 3. (Color online) Comparison of experimental and calculated Q_t for ^{102,104}Mo. There are two sets of experimental data - one from Ref. [43] (shown in green symbols) and the other from Ref. [44] (shown in red symbols).

The TPSM results obtained after configuration mixing are compared with the known experimental data for the studied even-even Mo- and Ru- isotopes in Fig. 2. For ^{102}Mo, the yrast band is experimentally known up to angular-momentum $I = 16$ and very few states have been observed for the γ-band. It is evident from Fig. 2 that TPSM reproduces the known experimental data reasonably well, in particular, the γ-bandhead energy which approximately lies at 1 MeV. There is no known data for the $\gamma\gamma$-band in this isotope and the TPSM predicts the bandhead of this band at $\sim$ 2 MeV excitation energy. For ^{104,106,108}Mo, the experimental data is quite rich, with both γ- and $\gamma\gamma$-

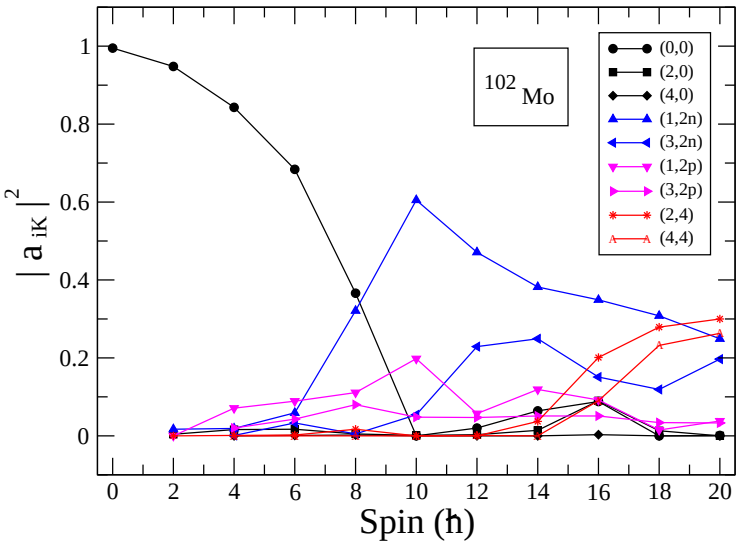

Fig. 4. (Color online) Probability of various projected K-configurations in the wave function of the Yrast band of ^{102}Mo. The labels (0,0), (2,0), (4,0), (1,2n), (3,2n), (1,2p), (3,2p), (2,4), and (4,4) correspond, respectively, to the configurations of ground, γ, 2γ, two neutron-aligned, γ-band built on this two neutron-aligned state, two proton-aligned, γ-band built on this two proton-aligned state, two-neutron plus two-proton aligned band, and γ band built on this four-qp state.

bands known up to quite high angular-momenta. It is quite evident from the comparison that TPSM reproduces the yrast-, γ-, and $\gamma\gamma$- bands surprisingly well. For ^{108}Mo, there is a clear discrepancy between the theory and the experimental energies of the $\gamma\gamma$-band. This problem has also been noted in the TPSM study of some other isotopes [27].

From the TPSM results of Ru-isotopes with $A = 108$ to 112, it is again evident from Fig. 2 that calculations reproduce the known experimental data quite well, especially for the known yrast- and γ-bands. γ-band. In ^{108}Ru these are known up to spin $I = 12$ and, on the other hand, only two states with $I = 4$ and 5 have been identified in the $\gamma\gamma$-band. For ^{110}Ru, γ-band is known up to $I = 13$ and no states in $\gamma\gamma$-band have been identified. Both γ- and $\gamma\gamma$-bands are known up to quite high spin in ^{112}Ru. The discrepancy in the bandhead energy of the $\gamma\gamma$-band is again noted for Ru-isotopes.

The Q_t transition probabilities have been evaluated using the expressions already given in our earlier publications [45,46]. As examples, the calculated Q_t transition probabilities for two Mo-isotopes are depicted in Fig. 3 (and for other Mo- and Ru-isotopes they have been discussed in Ref. [47]). The transitions were evaluated using the standard effective charges of $e_n = 0.5e$ and $e_p = 1.5$. The measured value of Q_t for $I = 2$ in Fig. 3 is from Ref. [43] and for other spin values is from the recent detailed lifetime analysis [44]. The drop in the BE2 transitions around $I = 8 - 10$ is noted for both the nuclei in Fig. 3 and these features are correctly described by the present TPSM calculations.

Table 2
Comparison of the known experimental γ-band Q_t values (in efm^2) and calculated ones for ^{102,104,108}Mo and ^{108,110}Ru isotopes.

$(I,K)_i \to (I,K)_f$	^{102}Mo	^{104}Mo	^{106}Mo	^{108}Ru	^{110}Ru
$(4,2)_i \to (2,2)_f$	188.82	237.56	151.38	197.27	210.06
$(5,2)_i \to (3,2)_f$	243.20	264.55	288.03	259.40	275.46
$(6,2)_i \to (4,2)_f$	236.62	312.84	296.15	253.71	273.54
Expt.					278^{+52}_{-37}
$(7,2)_i \to (5,2)_f$	270.50	298.74	229.99	296.68	305.57
Expt.					292^{+37}_{-31}
$(8,2)_i \to (6,2)_f$	245.36	329.45	209.13	312.42	283.06
Expt.		300^{+100}_{-80}		330^{+90}_{-70}	268^{+40}_{-31}
$(9,2)_i \to (7,2)_f$	154.19	266.53	297.07	309.98	310.51
Expt.		233^{+59}_{-34}	310^{+80}_{-80}		299^{+69}_{-48}
$(10,2)_i \to (8,2)_f$	185.66	330.83	312.88	327.14	278.46
Expt.		312^{+49}_{-42}		317^{+64}_{-55}	
$(11,2)_i \to (9,2)_f$	255.92	282.12	256.00	305.10	336.44
Expt.		267^{+30}_{-30}			
$(12,2)_i \to (10,2)_f$	315.20	324.98	314.55	326.81	268.33
$(13,2)_i \to (11,2)_f$	273.78	298.49	260.70	280.54	339.28
$(14,2)_i \to (12,2)_f$	254.59	317.68	258.33	354.90	90.82
$(15,2)_i \to (13,2)_f$	282.65	319.88	261.57	280.03	339.00
$(16,2)_i \to (14,2)_f$	273.83	115.91	268.77	370.64	365.87
$(17,2)_i \to (15,2)_f$	285.32	313.70	262.34	264.17	335.28
$(18,2)_i \to (16,2)_f$	216.05	396.70	267.72	372.42	369.11
$(19,2)_i \to (17,2)_f$	276.24	296.71	292.36	240.13	327.13
$(20,2)_i \to (18,2)_f$	321.25	430.03	297.30	373.71	370.38
$(4,2)_i \to (2,0)_f$	95.088	64.45	84.18	68.71	71.62
Expt.				$78^{+26.5}_{-26}$	
$(6,2)_i \to (4,0)_f$	98.34	44.81	96.34	52.43	46.81
$(8,2)_i \to (6,0)_f$	81.59	35.16	80.34	40.87	31.32
$(10,2)_i \to (8,0)_f$	57.53	24.31	85.11	50.83	22.94
$(12,2)_i \to (10,0)_f$	62.22	8.79	64.08	78.35	23.69
$(14,2)_i \to (12,0)_f$	53.11	12.68	37.11	89.88	46.55
$(16,2)_i \to (14,0)_f$	44.32	28.07	30.55	30.04	59.74
$(18,2)_i \to (16,0)_f$	34.89	29.59	26.95	52.69	61.92
$(20,2)_i \to (18,0)_f$	30.21	18.86	73.35	70.23	44.86

Table 3
Axial and triaxial quadrupole deformation parameters ϵ and γ (defined by $\tan^{-1}\gamma = \epsilon'/\epsilon$) employed in the TPSM calculation for odd-neutron Mo and Ru isotopes.

	^{103}Mo	^{105}Mo	^{107}Mo	^{109}Ru	^{111}Ru
ϵ	0.345	0.316	0.300	0.281	0.263
γ	23	20	30	22	23

In order to correlate the above observed behavior of Q_t with the structural changes along the yrast line, the projected K-configurations in the wave function of the yrast band are plotted in Fig. 4 for ^{102}Mo as an illustrative example. It can be seen that the yrast band up to $I = 6$ is dominated by the qp-vacuum configuration with $K = 0$, and above this spin value, it is noted that the two-quasineutron state with $K = 1$ becomes dominant and this change in the yrast band structure gives rise to the observed drop in the measured Q_t. It is also evident from Fig. 4 that above $I = 14$, four-qp configurations having $K = 2$ and 4 become important, which leads to further drop in Q_t with increasing spin. Thus the successive changes in the structure associated with spin alignments of nucleons roughly result in a 1/3 of reduction in collectivity of the yrast band at $I = 20$.

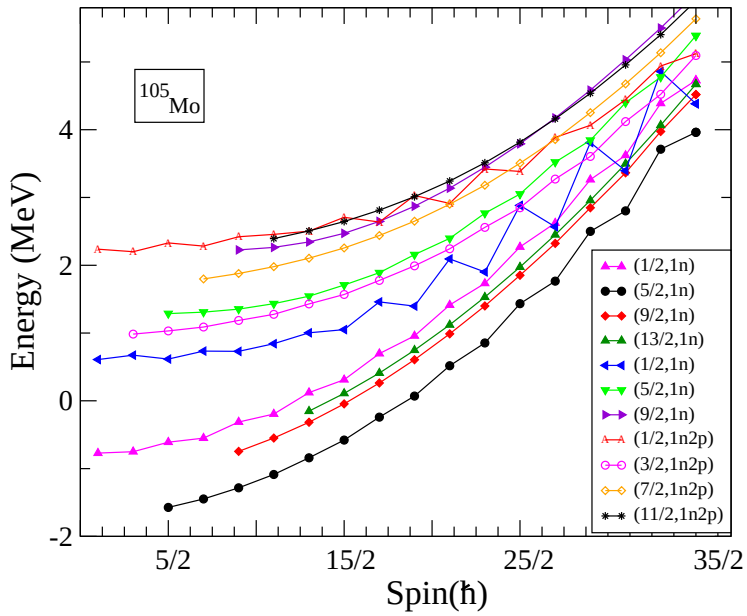

Fig. 5. (Color online) Band diagram for ^{105}Mo depicting the angular-momentum projected bands from one- and three-qp states. For clarity, only the lowest projected bands are shown and in the numerical calculations, projection has been performed from forty-four intrinsic states for this nucleus.

In Table 2, we show the calculated Q_t quadrupole transition moments along the γ-band. The inter-band transitions from the γ to the yrast-band are also shown. Previously inter-band transitions between the γ and the yrast-band were studied for some rare-earth nuclei in a smaller configuration space with-

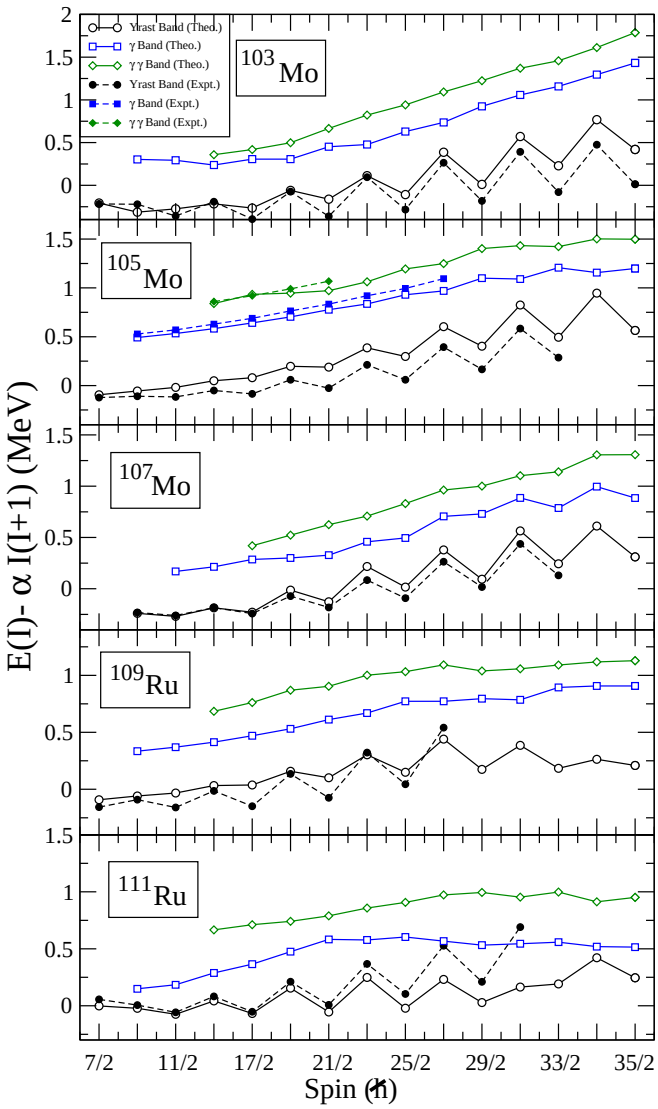

Fig. 6. (Color online) Comparison of the measured energy levels of Yrast- γ- and $\gamma\gamma$-Bands for ^{103,105,107}Mo and ^{109,111}Ru nuclei and the results of TPSM calculations. The scaling factor α appearing in the y-axis is defined as $\alpha = 32.32A^{-5/3}$. Data taken from Refs. [29,49].

out inclusion of qp excitations [23]. The experimental Q_t values known for some transitions are also depicted in Table 2. It is noted that these Q_t values are well reproduced by the TPSM calculation. Q_t transitions along the γ-band are noted to increase with increasing spin and the transition quadrupole moment for the odd-spin value is slightly smaller than for the even-spin value. It is found that the inter-band transitions are in general 3-5 times weaker than those in-band transitions, but still they are large enough to claim a similar collective structure of the γ-band as for the yrast-band.

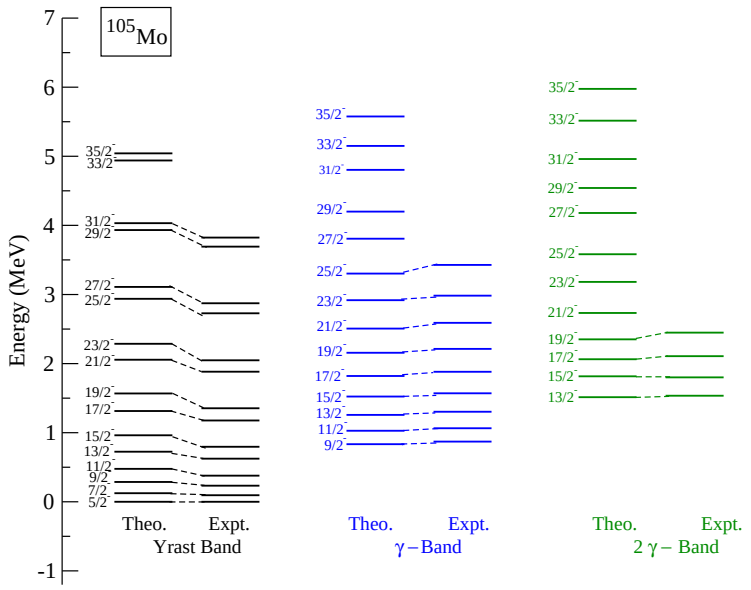

Fig. 7. (Color online) The calculated yrast-, γ-, and $\gamma\gamma$-bands of ^{105}Mo are compared with the corresponding experimental data [29].

3.2 Odd-neutron systems

The TPSM calculations have been performed for odd-neutron $^{103-105}$Mo and ^{109,111}Ru isotopes by using the same coupling parameters in the Hamiltonian (6) as for the even-even system. The configuration space consists of 1- and 3-qp states as given in (2). The axial and non-axial deformations used in this calculation are listed in Table 3. The axial deformations have been adopted from earlier studies on these nuclei [36,37,38,39,48]. The triaxial deformation ϵ', shown in the form of γ in Table 3, are chosen in such a way that the bandhead of the γ bands in these odd-neutron isotopes is reproduced.

In Fig. 5, we show the calculated band diagram for ^{105}Mo as the representative example for odd-neutron systems. The ground-state is the projected 1-qp state with $K = 5/2$. For odd-mass nuclei, there are two possible γ-bands with $K = K_g \pm 2$, where K_g is the K-value of the ground-state band. In Fig. 5, both these possible γ-bands with $K = 9/2$ and $1/2$ are displayed. Since the two γ-bands originate from the same intrinsic qp structure, the bandhead energies of them are roughly the same, as seen in Fig. 5. As a rule, the one with the larger K (here the $K = 9/2$ one) is energetically favored as the band starts to rotate at a higher spin (here from $I = 9/2$). $K = 1/2$ γ-band lies at a higher excitation energy for the entire spin regime as compared to the favored $K = 9/2$ band in Fig. 5. The splitting between these two bands is quite interesting and can provide a measure of the interaction between qp and collective degrees of freedom. The predicted $\gamma\gamma$-band lies between the $K = 9/2$ and $K = 1/2$ γ-bands and comes very close to the $K = 9/2$ γ-band for high-spin states.

Table 4
Predicted B(E2) values (in W.u.) for ^{103,105,107}Mo and ^{109,111}Ru isotopes.

$(I,K)_i \to (I,K)_f$	^{103}Mo	^{105}Mo	^{107}Mo	^{109}Ru	^{111}Ru
$(9/2,5/2)_i \to (5/2,5/2)_f$	10.10	12.36		11.05	8.38
$(11/2,5/2)_i \to (7/2,5/2)_f$	40.46	21.24	20.32	32.41	23.49
$(13/2,5/2)_i \to (9/2,5/2)_f$	60.10	42.97	50.30	62.84	49.05
$(15/2,5/2)_i \to (11/2,5/2)_f$	92.07	63.76	107.3	108.68	92.75
$(17/2,5/2)_i \to (13/2,5/2)_f$	119.77	98.97	100.57	80.62	90.36
$(19/2,5/2)_i \to (15/2,5/2)_f$	135.60	119.39	120.23	109.43	94.88
$(21/2,5/2)_i \to (17/2,5/2)_f$	149.69	134.77	145.71	101.01	101.37
$(23/2,5/2)_i \to (19/2,5/2)_f$	161.45	146.48	155.16	114.71	104.17
$(25/2,5/2)_i \to (21/2,5/2)_f$	160.37	145.45	156.67	110.31	100.60
$(27/2,5/2)_i \to (23/2,5/2)_f$	170.71	153.84	164.55	121.71	110.16
$(29/2,5/2)_i \to (25/2,5/2)_f$	168.65	152.95	165.36	106.31	99.80
$(31/2,5/2)_i \to (27/2,5/2)_f$	175.84	143.54	169.82	108.94	107.10
$(33/2,5/2)_i \to (29/2,5/2)_f$	174.98	142.72	171.30	98.86	90.63
$(35/2,5/2)_i \to (31/2,5/2)_f$	157.81	115.03	147.79	99.30	76.94
$(13/2,9/2)_i \to (9/2,9/2)_f$	42.08	36.67		13.93	21.81
$(15/2,9/2)_i \to (7/2,9/2)_f$	60.72	72.46	83.57	64.92	55.62
$(17/2,9/2)_i \to (13/2,9/2)_f$	119.77	115.32	103.42	101.09	84.57
$(19/2,9/2)_i \to (15/2,9/2)_f$	125.02	108.72	131.36	85.64	70.54
$(21/2,9/2)_i \to (17/2,9/2)_f$	134.69	123.55	111.32	83.11	75.82
$(23/2,9/2)_i \to (19/2,9/2)_f$	126.69	106.48	114.41	78.72	70.96
$(25/2,9/2)_i \to (21/2,9/2)_f$	147.43	129.68	132.83	98.59	89.73
$(27/2,9/2)_i \to (23/2,9/2)_f$	139.22	114.49	126.17	85.52	76.47
$(29/2,9/2)_i \to (25/2,9/2)_f$	155.79	125.54	146.49	111.11	85.44
$(31/2,9/2)_i \to (27/2,9/2)_f$	134.61	119.07	127.53	96.26	97.10
$(33/2,9/2)_i \to (29/2,9/2)_f$	125.32	112.03	129.99	105.52	80.63
$(35/2,9/2)_i \to (31/2,9/2)_f$	130.41	106.15	124.30	86.50	70.79
$(17/2,13/2)_i \to (13/2,13/2)_f$	43.97	42.46		22.43	25.27
$(19/2,13/2)_i \to (15/2,13/2)_f$	80.51	77.26	82.96	85.64	73.67
$(21/2,13/2)_i \to (17/2,13/2)_f$	133.60	125.70	149.51	97.29	87.52
$(23/2,13/2)_i \to (19/2,13/2)_f$	126.96	108.74	160.00	109.93	96.61
$(25/2,13/2)_i \to (21/2,13/2)_f$	146.53	138.63	149.62	98.21	87.94
$(27/2,13/2)_i \to (23/2,13/2)_f$	136.78	120.82	117.85	93.71	76.47
$(29/2,13/2)_i \to (25/2,13/2)_f$	124.02	140.48	121.05	100.13	97.91
$(31/2,13/2)_i \to (27/2,13/2)_f$	147.74	124.89	136.08	87.11	80.34
$(33/2,13/2)_i \to (29/2,13/2)_f$	150.57	130.73	147.80	85.52	87.04
$(35/2,13/2)_i \to (31/2,13/2)_f$	134.59	91.14	142.43	70.50	78.62

The results of TPSM calculations after configuration mixing are compared with the known experimental data in Fig. 6, where the yrast-, γ-, and $\gamma\gamma$-bands are shown. While there exist experimental data for the yrast band for every isotope up to quite high spin, the data for the γ- and $\gamma\gamma$-bands are known only for ^{105}Mo for which the TPSM calculations are noted to reproduce the data reasonably well. In particular, the bandheads of both γ- and $\gamma\gamma$-bands

are described correctly. The TPSM calculations again predict two γ-bands with $K = 1/2$ and $9/2$ but we show only the one with the larger K-value. The observed yrast bands for all the studied odd-neutron systems clearly depict signature splitting that increases with increasing angular momentum. This splitting is well reproduced for all the nuclei in Fig. 6 except for ^{109}Ru where discrepancy is clearly noted, in particular, for the low spin states. To have a better comparison between the data and the TPSM calculations, yrast-, the level energies of γ-, and $\gamma\gamma$-bands are compared in Fig. 7 for ^{105}MO. It is quite evident from this figure that comparison between the TPSM calculated energies and the experimental data is quite satisfactory.

To make the study complete, the calculated B(E2) values for the studied odd-neutron isotopes are depicted in Table. 4. Presently, there is no data available for a comparison. The predicted in-band transitions show a similar behavior for all the studied nuclei with increasing trend as a function of angular-momentum. The general trend is that Ru isotopes show relatively smaller B(E2) values as compared to Mo, in particular, for the high spin states and this corresponds to smaller deformation values for Ru isotopes. It is also evident that for a given nucleus, the γ- and $\gamma\gamma$-bands have slightly weaker collectivity than the corresponding yrast one. Experimental confirmation for these predictions are very much desired.

4 Summary and Conclusions

In the present work a systematic analysis of the band structures observed in neutron-rich Mo- and Ru-isotopes has been performed using the recently developed multi-qp TPSM approach. In this mass region, rich band structures have been observed and this is one of the few regions where γ- and $\gamma\gamma$-bands have been observed up to quite high-spin. The advantage of the TPSM approach is that it provides a unified microscopic description of the collective and the qp excitation modes. It has been demonstrated that, in general, TPSM results are in good agreement with the available experimental data for energy levels and transitions. Among them ^{105}Mo is the only known odd-mass system where well developed γ- and $\gamma\gamma$-bands have been observed and it has been shown that TPSM approach provides a satisfactory description of the known band structures for this isotope. However, there appears to be a problem to reproduce the bandhead of the $\gamma\gamma$-band for many nuclei studied in this work and this problem was also noted in our earlier investigation for ^{103}Nb [27]. A possible reason for this discrepancy could be that $\gamma\gamma$-band is having considerable mixing from the vibrational degree of freedom for cases where large disagreement is noted. A possible way to include the vibrational mode is by superimposing different γ-deformed solutions in the spirit of projected generator coordinate method [50]. This may provide a resolution to this problem

and also may help improve the overall description of the nuclear spectroscopic quantities using the TPSM approach.

Acknowledgments

The authors would like to acknowledge W. Nazarewicz for his encouragement during the course of this work. Research at SJTU was supported by the National Natural Science Foundation of China (Nos. 11575112, 11135005), by the 973 Program of China (No. 2013CB834401), and by the Open Project Program of the State Key Laboratory of Theoretical Physics, Institute of Theoretical Physics, Chinese Academy of Sciences, China (No. Y5KF141CJ1).

References

[1] A. Bohr and B. R. Mottelson, *Nuclear Structure*, Vol. II (Benjamin Inc., New York, 1975).

[2] V. G. Soloviev and N. Yu. Shirikova, Z. Phys. **A 301** (1981) 263.

[3] A. Bohr and B. R. Mottelson, Phys. Scr. **25** (1982) 28.

[4] H.G. Borner, J. Jolie, S.J. Rabinson, B. Krusche, R. Piepenring, R.F. Lasten, A. Aprahamian, J.P. Draayer, Phys. Rev. Lett. **66** (1991) 691.

[5] J.H. Hamilton, A.V. Ramayya, S.J. Zhu, G.M. Ter-Akopian, Yu. Ts. Oganessian, J.D. Cole, J.O. Rasmussen, M.A. Stoyer, Prog. Part. Nucl. Phys. **35**, 635 (1995).

[6] S.J. Zhu, Y.X. Luo, J.H. Hamilton, J.O. Rasmussen, A.V. Ramayya, J.K. Hwang, H.B. Ding, X.L. Che, Z. Jiang, P.M. Gore, E.F. Jones, K. Li, I.Y. Lee, W.C. Ma, G.M. Ter-Akopian, A.V. Daniel, S. Frauendorf, V. Dimitrov, J.Y. Zhang, A. Gelberg, I. Stefancescu, J.D. Cole, Prog. Part. Nucl. Phys. **59** (2007) 329.

[7] W. Urban, T. Rzaca-Urban, J.L. Durell, W.R. Phillips, A.G. Smith, B.J. Varley, I. Ahmad, N. Schulz, Eur. Phys. J. A **20** (2004) 381.

[8] S.J. Zhu, J.H. Hamilton, A.V. Ramayya, P.M. Gore, J.O. Rasmussen, V. Dimitrov, S. Frauendorf, R.Q. Xu, J.K. Hwang, D. Fong, L.M. Yang, K. Li, Y.J. Chen, X.Q. Zhang, E.F. Jones, Y.X. Luo, I.Y. Lee, W.C. Ma, J.D. Cole, M.W. Drigert, M. Stoyer, G.M. Ter-Akopian, A.V. Daniel, Eur. Phys. J. A **25** (2005) Suppl. 1, 459.

[9] S.J. Zhu, J.G. Wang, L. Gu, J.H. Hamilton, A.V. Ramayya, Y.X. Luo, J.O. Rasmussen, J.K. Hwang, H.B. Ding, K. Li, S.H. Liu, E.Y. Yeoh, Q. Xu, Z.G. Xiao, Sci China-Phys Mech Astron **54** (2011) Suppl. 1, s44.

[10] A. Guessous, N. Schulz, W.R. Phillips, I. Ahmad, M. Bentaleb, J.L. Durell, M.A. Jones, M. Leddy, E. Lubkiewicz, L.R. Morss, R. Piepenbring, G. Smith, W. Urban, B.J. Varley, Phys. Rev. Lett. **75** (1995) 2280.

[11] A. Guessous, N. Schulz, M. Bentale, E. Lubkiewicz, J.L. Durell, C.J. Pearson, W.R. Phillips, J.A. Shannon, W. Urban, B.J. Varley, I. Ahmad, C.J. Lister, L.R. Morss, K.L. Nash, C.W. Williams, S. Khazrouni, Phys. Rev. C **53** (1996) 1191.

[12] H. Hua, C.Y. Wu, D. Cline, A.B. Hayes, R. Teng, R.M. Clark, P. Fallon, A. Goergen, A.O. Macchiavelli, K. Vetter, Phys. Rev. C **69** (2004) 014317.

[13] L.M. Yang, S.-J. Zhu, K. Li, J.H. Hamilton, A.V. Ramayya, J.K. Hwang, X.Q. Zhang, L.Y. Zhu, C.-Y. Gan, M. Sakhaee, G.-L. Long, R.-Q. Xu, Z. Zhang, Z. Jiang, J. Myong-Gil, W.C. Ma, B.R.S. Babu, J. Komicki, E.F. Jones, J.D. Cole, R. Aryaeinejad, M.W. Drigert, I.Y. Lee, J.O. Rasmussen, M.A. Stoyer, G.M. Ter-Akopian, A.V. Daniel, Chin. Phys. Lett. **18** (2001) 24.

[14] M.A.C. Hotchkis et al., Nucl. Phys. A **530** (1991) 111.

[15] S. Zhu et al., Rev. Mex. Fis. **38** (1992) Suppl., 53.

[16] P. Moller, J.R. Nix, W.D. Myers, W.J. Swiatecki, At. Data Nucl. Data Tables **59** (1995) 185.

[17] J. Skalski, S. Mizutori, W. Nazarewicz, Nucl. Phys. A **617** (1997) 282.

[18] G.A. Lalazissis, S. Raman, P. Ring, At. Data Nucl. Data Tables **71** (1999) 1.

[19] J.A. Sheikh and K. Hara, Phys. Rev. Lett. **82** (1999) 3968.

[20] Y. Sun, K. Hara, J.A. Sheikh, J.G. Hirsch, V. Velazquez, M. Guidry, Phys. Rev. C **61** (2000) 064323.

[21] J.A. Sheikh, Y. Sun, R. Palit, Phys. Lett. B **507** (2001) 115.

[22] Y. Sun, J.A. Sheikh, G.-L. Long, Phys. Lett. B **533** (2002) 253.

[23] P. Boutachkov, A. Aprahamian, Y. Sun, J.A. Sheikh, S. Frauendorf, Eur. Phys. J. A **15** (2002) 455.

[24] Y. Sun, G.-L. Long, F. Al-Khudair, J.A. Sheikh, Phys. Rev. C **77** (2008) 044307.

[25] J.A. Sheikh, G.H. Bhat, Y. Sun, G.B. Vakil, R. Palit, Phys. Rev. C **77** (2008) 034313.

[26] J.A. Sheikh, G.H. Bhat, R. Palit, Z. Naik, Y. Sun, Nucl. Phys. A **824** (2009) 58.

[27] J.A. Sheikh, G.H. Bhat, Y. Sun, R. Palit, Phys. Lett. B **688** (2010) 305.

[28] P. Möller, R. Bengtsson, B.G. Carlsson, P. Olivius, T. Ichikawa, Phys. Rev. Lett. **97** (2006) 162502.

[29] H.B. Ding, S.J. Zhu, J.H. Hamilton, A.V. Ramayya, J.K. Hwang, K. Li, Y.X. Luo, J.O. Rasmussen, I.Y. Lee, C.T. Goodin, X.L. Che, Y.J. Chen, M.L. Li, Phys. Rev. C **74** (2006) 054301.

[30] H. Hua, C.Y. Wu, D. Cline, A.B. Hayes, R. Teng, R.M. Clark, P. Fallon, A.O. Macchiavelli, K. Vetter, Phys. Rev. C **65** (2002) 064325.

[31] P. Ring and P. Schuck, *The Nuclear Many-Body Problem* (Springer, New York, 1980).

[32] K. Hara and Y. Sun, Int. J. Mod. Phys. E **4** (1995) 637.

[33] S.G. Nilsson, C.F. Tsang, A. Sobiczewski, Z. Szymanski, S. Wycech, C. Gustafson, I. Lamm, P. Moller, B. Nilsson, Nucl. Phys. A **131** (1969) 1.

[34] E. Y. Yeoh, S. J. Zhu, J. H. Hamilton, K. Li, A. V. Ramayya, Y. X. Liu, J. K. Hwang, S. H. Liu, J. G. Wang, Y. Sun, J. A. Sheikh, G. H. Bhat, Y. X. Luo, J. O. Rasmussen, I. Y. Lee, H. B. Ding, L. Gu, Q. Xu, Z. G. Xiao, W. C. Ma, Phys. Rev. C **83** (2011) 054317.

[35] P. Möller, J. R. Nix, W. D. Myers, and W. J. Swiatecki, At. Data Nucl. Data Tables **59** (1995) 185.

[36] H. Bohn et al., Z. Phys. A **274** (1975) 327.

[37] J. A. Pinston, W. Urban, Ch. Droste, T. Rzaca-Urban, J. Genevey, G. Simpson, J. L. Durell, A. G. Smith, B. J. Varley, I. Ahmad, Phys. Rev. C **74** (2006) 064304.

[38] Q. H. Lu et al., Phys. Rev. C **52** (1995) 1348.

[39] C. Y. Wu, H. Hua, D. Cline, A. B. Hayes, R. Teng, D. Riley, R. M. Clark, P. Fallon, A. Goergen, A. O. Macchiavelli, K. Vetter, Phys. Rev. C **73** (2006) 034312.

[40] K. Hara and Y. Sun, Nucl. Phys. A **529** (1991) 445.

[41] X. L. Che, S. J. Zhu, J. H. Hamilton, A. V. Ramayya, J. K. Hwang, U. Yong-Nam, M. L. Li, R. C. Zheng, I. Y. Lee, J. O. Rasmussen, Y. X. Luo, W.C. Ma, Chin. Phys. Lett. **21** (2004) 1904.

[42] E. S. Jones, et al., Phys. of Atomic Nuclei, **69** (2006) 7.

[43] S. Raman, C. H. Malarkey, W. T. Milner, C. W. Nestor, Jr., P. H. Stelson, Atom. Data Nucl. Data Tables **36** (1987) 1.

[44] J. B. Snyder, W. Reviol, D. G. Sarantites, A. V. Afanasjev, R. V. F. Janssens, H. Abusara *et al.*, Phys. Lett. B **723** (2013) 61.

[45] G. H. Bhat, W. A. Dar, J. A. Sheikh, Y. Sun, Phys. Rev. C **89** (2014) 014328.

[46] G. H. Bhat, J. A. Sheikh, R. Palit, Phys. Lett. B **707** (2012) 250.

[47] C. L. Zhang, G.H. Bhat, W. Nazarewicz, J. A. Sheikh and Y. Shi, Phys. Rev. C **92** (2015) 034307.

[48] M. Liang et al., Z. Phys. A **346** (1993) 101.

[49] J. K. Hwang, A. V. Ramayya, J. H. Hamilton, L. K. Peker, J. Kormicki, B. R. S. Babu, T. N. Ginter, C. J. Beyer, G. M. Ter-Akopian, Yu. Ts. Oganessian, A. V. Daniel, W. C. Ma, P. G. Varmette, J. O. Rasmussen, S. J. Asztalos, S. Y. Chu, K. E. Gregorich, A. O. Macchiavelli, R. W. Macleod, J. Gilat, J. D. Cole, R. Aryaeinejad, K. Butler-Moore, M. W. Drigert, M. A. Stoyer, L. A. Bernstein, R. W. Lougheed, K. J. Moody, S. G. Prussin, H. C. Griffin, R. Donangelo, J. Phys. G **24** (1998) L9.

[50] F.-Q. Chen, Y. Sun, P. Ring, Phys. Rev. C **88** (2013) 014315.